Research Article

EXPERIMENTAL AND QUANTUM CHEMICAL STUDIES ON MOLECULAR STRUCTURE, SPECTROSCOPIC ANALYSIS, NLO ANALYSIS AND HOMO-LUMO OF SUBSTITUTED N-FERROCENYLMETHYL-N-PHENYLAMIDES

N. Zegheb[1], C. Boubekri[1,2*], T. Lanez[1], A. Kerassaa[1]

[1]University of El Oued, VTRS Laboratory, B.P.789, 39000, El Oued, Algeria

[2]University of Biskra, Faculty of Exact Sciences, Natural and Lile Sciences, Department of Material Sciences, BP145 RP Biskra 07000 Algeria

ABSTRACT

This work aims to determine structural, crystal properties and molecular spectroscopy of three N-ferrocenylmethyl-N-phenylamide using DFT method. The computed bond lengths, bond angles and dihedral angles of the titled molecules were calculated and compared with the experimental geometrical parameters, the amount of positive and negative charges using Mulliken charge and the molecular electrostatic potential map (MESP) were also investigated. The theoretical vibrational frequencies were compared with the corresponding experimental data. ^1H and ^{13}C NMR spectra were obtained using gauge including atomic orbital (GIAO) method, the calculated and experimental chemical shifts were compared. The dipole moment, linear polarizability and first order hyperpolarizability values were also computed. A study on the electronic properties, HOMO and LUMO energies, were performed by time-dependent DFT (TD-DFT) approach.

Keywords: ferrocenic derivatives, DFT computational method, HOMO and LUMO energies, FT-IR, NMR, NLO properties.

Author Correspondence, e-mail: cherifa.boubekri@univ-biskra.dz

1. INTRODUCTION

Ferrocene [1] stands behind the tremendous growth of organometallic chemistry because of its fascinating sandwich structure. During the last decades, interest in ferrocene derivatives, in theoretical research just as in applied fields, has developed. They have various applications in materials science, medicine [2], organic synthesis [3], bio-organometallic and biological chemistry [4], asymmetric catalysis, nonlinear optics [5, 6], in polymer science as redox active polymers and dendrimers [7], in molecular recognition as biosensors [8-12] and in electrochemistry [13].

In this paper, we carry out a study of the molecular structure of three substituted N-ferrocenylmethylamides named N-ferrocenylmethyl-N-phenylacetamide (FPA), N-ferrocenylmethyl-N-phenylpropionamide (FPP) and N-ferrocenylmethyl-N-phenylbenzamide (FPB) using Density Functional Theory (DFT) method.

2. EXPERIMENTAL

The synthesis of FPA, FPP and FPB were achieved following our previously reported procedure [14-16]. The FT-IR of the compounds have been recorded using Nicolet iS5, Thermo Fisher Scientific spectrometer in the spectral region of 4000-400 cm^{-1}.

2.1. Quantum chemical calculations

All calculations were performed using Gaussian 09 software [17], the geometries were fully optimized by the DFT/ Becke's three parameter hybrid model with the Lee–Yang–Parr correlation functional (B3LYP) method with the 6-311++G(d,p) and LanL2DZ basis sets without imposing any symmetry constraints. These methods were also used to compute optimized structural geometrical parameters, Mulliken charge, hyperpolarizability, polarizability and dipole moment. Frequency calculations were employed to confirm the structure as minimum points in energy. At the optimized structure, no imaginary wavenumber modes were obtained. FT-IR spectra were obtained, the nuclear magnetic resonance spectra, ^{13}C and ^{1}H NMR, were calculated by the method of the gauge-independent atomic orbital (GIAO).

All spectra were obtained from computational methods of DFT / B3LYP with 6-311 ++ G (d,p) and LanL2DZ. Finally, the HOMO and LUMO values were obtained using time-dependent DFT (TD-DFT) with the same basis sets.

3. RESULTS AND DISCUSSION

3.1. Molecular geometry

The structures of FPA, FPP and FPB were optimized and the calculated geometric parameters were compared with the experimental values obtained from X-ray experiments [14-16], Tables 1, 2 and 3. The obtained results indicated that there is a good agreement between experimental and computational geometric parameters.

The Fe-C bond lengths were equal to 2.08 for ferrocene [18], also Mauricio. Y et al have found that this bond is equal to 2.08 for 2-ferrocenyl-1,8-naphthyridine complex [19]. In this work, the calculated Fe-C bond ranges from 2.070 to 2.079 Å using 6-311++G(d, p) and from 2.120 to 2.115 Å using LanL2DZ, while the experimental [14-16] vary from 1.99 to 2.08 Å with max difference equal to 0.08 Å using 6-311++G(d,p) and 0.13 Å using LanL2DZ. The calculated C-C bond lengths were in the range 1.53 to 1.39 Å and 1.53-1.40 Å using 6-311++G(d,p) and LanL2DZ respectively, these values are in good agreement with the experimental values which ranges from 1.52 Å to 1.37 Å. Mauricio et al. [19] have calculated this bond at 1.416 Å for similar ferrocene derivatives, and another study has shown that the C-C bond of ferrocene is equal to 1.39 Å [18]. Moreover, the C-N and C-O bonds were in the range of 1.37 to 1.49 Å and 1.22-1.26 Å for both basis set, respectively.

The expected value for bond angle in benzene ring is 120° [20, 21]. Likewise, in this work the C-C-C angles for benzene ring are from 117° to 120°. Moreover, the bond angles C6-C10-C11 of the studied compounds were calculated around 126° using both basis sets, whereas, the same angle were equal to 125.8° for 2-ferrocenyl-1,8-naphthyridine [19]. Besides, the torsional angles fit to the experimental values, e.g. the dihedral angle C6—C10—C11—N for FPA and FPP were equal to 76.72 (81.34) and -96.99 (81.444) using 6-311++G(d, p) (LanL2DZ) while the experimental values were equal to 93.3 and -96, respectively.

As seen from Tables 1, 2 and 3, most of the optimized bond lengths are slightly longer than the experimental values, and the bond angles are slightly different from experimental ones because the molecular states are different during experimental and theoretical processes.

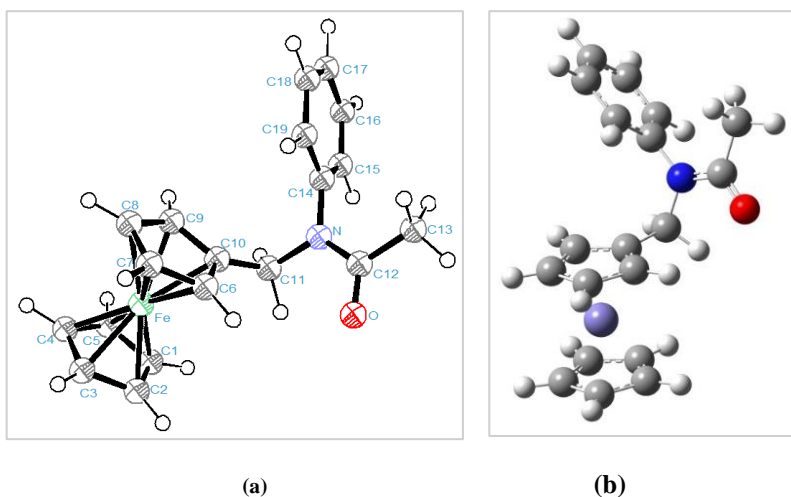### 3.1.1. N-ferrocenylmethyl-N-phenylacetamide (FPA)

Fig.1 (a) The ORTEP view of FPA shows atomic labeling scheme and 40% probability level displacement ellipsoids. **(b)** DFT optimized structure of FPA by GaussView

Table 1. Selected optimized and experimental geometry parameters of compound FPA by DFT/B3LYP method

FPA		X-Ray	a	b			X-Ray	a	b
Bond distances(Å)									
C1	Fe	2.05	2.077	2.12073	C18	H18	0.931	1.08421	1.08726
C2	Fe	2.056	2.0767	2.11937	C19	H19	0.929	1.08359	1.08689
C3	Fe	2.04	2.0766	2.1183	C1	H1	0.93	1.07983	1.08136
C4	Fe	2.03	2.078	2.12031	C1	C5	1.43	1.4265	1.44363
C5	Fe	1.99	2.0782	2.12141	C1	C2	1.37	1.42587	1.44299
C6	Fe	2.03	2.07377	2.11569	C2	C3	1.48	1.426	1.44321
C7	Fe	2.03	2.07648	2.11778	C3	C4	1.44	1.426	1.44336
C8	Fe	2.03	2.07454	2.11507	C4	C5	1.40	1.4259	1.44299
C9	Fe	2.088	2.0729	2.11403	C10	C11	1.52	1.50396	1.50754
C10	Fe	2.002	2.07368	2.11939	C6	C7	1.42	1.4246	1.44101
C4	H4	0.93	1.0797	1.08126	C6	C10	1.40	1.43121	1.44557
C3	H3	0.931	1.0796	1.08113	C7	C8	1.38	1.42688	1.44429
C2	H2	0.93	1.0795	1.08102	C8	C9	1.49	1.42541	1.44231
C5	H5	0.93	1.0797	1.0813	C9	C10	1.47	1.43073	1.44486
C6	H6	0.93	1.07964	1.08093	C12	C13	1.509	1.51855	1.52342
C7	H7	0.93	1.07988	1.0811	C14	C19	1.372	1.39667	1.40957
C8	H8	0.93	1.07989	1.08114	C14	C15	1.374	1.39772	1.41032
C9	H9	0.93	1.0804	1.08174	C15	C16	1.385	1.39309	1.40713
C11	H11b	0.97	1.09228	1.09625	C16	C17	1.368	1.39467	1.40919
C11	H11a	0.97	1.08876	1.09351	C17	C18	1.366	1.39376	1.40857
C13	H13a	0.96	1.08857	1.09218	C18	C19	1.376	1.39402	1.40734
C13	H13b	0.959	1.0908	1.09499	C12	O	1.225	1.22372	1.2619
C13	H13c	0.96	1.09357	1.0972	C12	N	1.359	1.37948	1.38997
C15	H15	0.931	1.08445	1.08752	C14	N1	1.435	1.43442	1.44447
C16	H16	0.93	1.08422	1.08736	N1	C11	1.479	1.48051	1.49374

					regression coefficients (R2)			0.9801	0.9797
C17	H17	0.929	1.08409	1.0873					
Bond angles (°)									
H1	C1	C2	126.01	125.915	125.922	H13b	C13	C12	109.47	112.782	112.253
H1	C1	C5	125.98	126.044	126.06	H13a	C13	H13c	109.44	108.545	108.604
H1	C1	Fe	125.81	124.96	125.433	H13a	C13	C12	109.48	107.657	107.842
C2	C1	C5	108	108.034	108.018	H13c	C13	C12	109.49	110.093	110.585
C2	C1	Fe	70.33	69.907	70.053	C19	C14	C15	119.39	119.612	119.86
C5	C1	Fe	69.41	69.962	70.13	C19	C14	N	120.76	120.579	120.394
H2	C2	C3	126.25	126.05	126.049	C15	C14	N	119.81	119.788	119.728
H2	C2	C1	126.14	125.969	125.971	H15	C15	C14	120.26	119.206	119.272
H2	C2	Fe	126	124.58	124.851	H15	C15	C16	120.23	120.603	120.671
C3	C2	C1	107.61	107.965	107.976	C14	C15	C16	119.51	120.188	120.056
C3	C2	Fe	70.04	69.916	70.049	H16	C16	C17	119.57	120.128	120.057
C1	C2	Fe	69.36	69.942	70.154	H16	C16	C15	119.57	119.778	119.846
H3	C3	C4	125.6	125.984	125.992	C17	C16	C15	120.85	120.094	120.096
H3	C3	C2	125.54	125.971	125.978	H17	C17	C18	120.39	120.104	120.11
H3	C3	Fe	126.4	124.646	124.826	H17	C17	C16	120.3	120.08	120.079
C4	C3	C2	108.87	108.031	108.027	C18	C17	C16	119.31	119.816	119.81
C4	C3	Fe	69.79	69.979	70.166	H18	C18	C17	119.9	120.099	120.07
C2	C3	Fe	69.83	69.921	70.128	H18	C18	C19	119.81	119.701	119.735
H4	C4	C3	126.05	126.009	126.016	C17	C18	C19	120.29	120.199	120.194
H4	C4	C5	126.14	125.984	125.995	H19	C19	C14	119.6	119.259	119.292
H4	C4	Fe	126.12	124.806	125.034	H19	C19	C18	119.79	120.656	120.725
C3	C4	C5	107.8	107.996	107.987	C14	C19	C18	120.61	120.084	119.98
C3	C4	Fe	70.21	69.869	70.016	C12	N	C14	124.16	123.423	123.455
C5	C4	Fe	69.23	69.94	70.152	C12	N	C11	118.7	118.461	118.356
H5	C5	C4	126.19	125.983	125.959	C14	N	C11	116.9	117.84	117.97
H5	C5	C1	126.09	126.035	126.049	C9	Fe	C5	107.14	109.036	109.814
H5	C5	Fe	125.44	124.995	125.425	C9	Fe	C10	41.06	40.368	39.912
C4	C5	C1	107.72	107.975	107.992	C9	Fe	C6	68.28	67.614	66.956
C4	C5	Fe	70.3	69.931	70.071	C9	Fe	C1	128.95	124.415	124.799
C1	C5	Fe	69.73	69.883	70.079	C9	Fe	C4	116.55	123.554	124.311
H6	C6	C10	125.88	124.989	124.773	C9	Fe	C7	67.68	67.524	66.923
H6	C6	C7	126.06	126.768	127.042	C9	Fe	C8	40.21	40.203	39.881
H6	C6	Fe	125.94	125.099	125.622	C9	Fe	C2	167.78	159.941	159.85
C10	C6	C7	108.06	108.236	108.183	C9	Fe	C3	149.97	158.706	159.178
C10	C6	Fe	69.61	69.81	70.18	C5	Fe	C10	114.86	123.542	124.51
C7	C6	Fe	70.04	70.027	70.178	C5	Fe	C6	148.28	158.999	159.549
H7	C7	C8	125.9	125.938	125.988	C5	Fe	C1	40.86	40.155	39.791
H7	C7	C6	126.01	125.948	125.961	C5	Fe	C4	40.46	40.129	39.777
H7	C7	Fe	126.57	124.587	124.996	C5	Fe	C7	168.53	159.704	159.553
C8	C7	C6	108.09	108.089	108.046	C5	Fe	C8	129.53	124.196	124.513
C8	C7	Fe	69.97	69.822	69.948	C5	Fe	C2	68.19	67.492	66.836
C6	C7	Fe	69.11	69.822	70.021	C5	Fe	C3	67.61	67.468	66.834
H8	C8	C9	126.01	126.042	126.049	C10	Fe	C6	40.68	40.374	39.916
H8	C8	C7	125.91	126.048	126.083	C10	Fe	C1	106.72	108.535	109.493
H8	C8	Fe	126.45	124.619	125.018	C10	Fe	C4	148.32	159.094	159.695
C9	C8	C7	108.08	107.894	107.867	C10	Fe	C7	68.53	67.771	66.979
C9	C8	Fe	69.17	69.836	70.021	C10	Fe	C8	68.57	67.863	67.077
C7	C8	Fe	69.95	69.968	70.151	C10	Fe	C2	129.41	123.662	124.118
H9	C9	C8	125.56	126.032	126.123	C10	Fe	C3	168.82	159.31	159.181
H9	C9	C10	125.55	125.619	125.623	C6	Fe	C1	116.25	123.226	123.991
H9	C9	Fe	125.81	124.825	125.426	C6	Fe	C4	170.27	159.21	159
C8	C9	C10	108.88	108.333	108.254	C6	Fe	C7	40.85	40.151	39.801
C8	C9	Fe	70.62	69.961	70.098	C6	Fe	C8	68.21	67.618	66.994

C10	C9	Fe	69.65	69.845	70.244	C6	Fe	C2	109.34	108.094	108.763
C6	C10	C9	106.88	107.446	107.649	C6	Fe	C3	132	123.37	123.591
C6	C10	C11	126.28	125.794	125.523	C1	Fe	C4	68.1	67.459	66.819
C6	C10	Fe	69.71	69.817	69.904	C1	Fe	C7	150.28	158.418	158.856
C9	C10	C11	126.81	126.722	126.824	C1	Fe	C8	167.64	160.115	160.041
C9	C10	Fe	69.28	69.787	69.844	C1	Fe	C2	40.31	40.152	39.793
C11	C10	Fe	124.61	127.422	126.201	C1	Fe	C3	67.5	67.468	66.836
H11a	C11	H11b	107.71	108.769	109.028	C4	Fe	C7	131.46	123.676	123.884
H11a	C11	N	108.97	106.331	106.363	C4	Fe	C8	109.49	108.482	109.103
H11a	C11	C10	108.97	110.443	110.382	C4	Fe	C2	67.81	67.489	66.859
H11b	C11	N	108.93	107.701	107.593	C4	Fe	C3	40	40.152	39.818
H11b	C11	C10	108.99	110.206	110.475	C7	Fe	C8	40.08	40.21	39.901
N	C11	C10	113.13	113.216	112.836	C7	Fe	C2	118.96	122.758	123.385
O	C12	N	120.99	121.565	121.081	C7	Fe	C3	111.35	108.009	108.553
O	C12	C13	121.32	121.248	121.354	C8	Fe	C2	151.25	158.266	158.668
N	C12	C13	117.69	117.187	117.564	C8	Fe	C3	119.06	122.928	123.55
H13b	C13	H13a	109.49	110.154	109.922	C2	Fe	C3	40.12	40.163	39.823
H13b	C13	H13c	109.46	107.547	107.584	**regression coefficients (R^2)**				0.9899	0.9892
Dihedral angles (°)											
C19—C14—N—C12			110.5	79.317	79.33	Fe—C7—C6—C10			-59.4	-59.576	-60.147
C15—C14—N—C12			-71.6	-102.365	-102.189	C8—C7—C6—Fe			59.3	59.559	59.858
C19—C14—N—C11			-75.3	-94.55	-95.208	C6—C10—C9—C8			0	0.335	0.102
C15—C14—N—C11			102.6	83.768	83.273	C11—C10—C9—C8			-178.3	-178.184	-179.216
C14—N—C12—O1			173.5	174.463	174.789	Fe1—C10—C9—C8			-59.9	-59.592	-60.045
C11—N—C12—O			-0.6	-0.632	-0.27	C6—C10—C9—Fe			59.9	59.926	59.943
C14—N—C12—C13			-7	-5.82	-5.448	C11—C10—C9—Fe			-118.4	-122.224	-120.74
C12—N—C11—C10			-92.1	-94.456	-93.479	C4—C3—C2—C1			0.4	0.008	0.03
C15-C16-C17-C18			-1.6	-0.316	-0.315	Fe—C3—C2—C1			59.4	59.838	60.167
C14—N—C11—C10			93.3	79.722	81.343	C4—C3—C2—Fe			-59.1	-59.845	-60.197
C6—C10—C11—N			93.3	78.43	78.266	C10—C9—C8—C7			-0.1	-0.346	-0.076
C9—C10—C11—N			-88.7	-99.04	-100.935	Fe—C9—C8—C7			-59.4	-59.866	-60.212
Fe—C10—C11—N			-177.6	-169.354	-168.229	C10—C9—C8—Fe			59.3	59.52	60.136
C15-C14-C19-C18			-1.7	-0.99	-0.698	C6—C7—C8—C9			0.1	0.224	0.226
N—C14—C19—C18			176.3	179.31	179.177	Fe—C7—C8—C9			58.9	59.784	60.13
C19-C14-C15-C16			0.3	0.705	0.47	C6—C7—C8—Fe			-58.8	-59.559	-59.904
N—C14—C15—C16			-177.7	-179.039	-178.959	C2—C3—C4—C5			-0.2	-0.02	-0.035
C17-C16-C15-C14			1.3	0.054	0.036	Fe—C3—C4—C5			-59.2	-59.789	-60.138
C14-C19-C18-C17			1.4	0.626	0.421	C2—C3—C4—Fe			59.1	59.809	60.173
C11—N—C12—C13			178.9	179.652	179.967	C1—C5—C4—C3			-0.1	-0.024	-0.026
C19-C18-C17-C16			0.3	0.03	0.086	Fe—C5—C4—C3			59.8	59.745	60.052
C9—C10—C6—C7			0.1	0.195	0.241	C1—C5—C4—Fe			-59.9	-59.769	-60.078
C11—C10—C6—C7			178.4	178.071	179.087	C3—C2—C1—C5			-0.4	-0.007	-0.014
Fe—C10—C6—C7			59.7	59.712	60.146	Fe—C2—C1—C5			59.4	59.815	60.114
C9—C10—C6—Fe			-59.6	-59.907	-59.905	C3—C2—C1—Fe			-59.8	-59.821	-60.1
C11—C10—C6—Fe			118.7	122.217	120.766	C4—C5—C1—C2			0.3	0.019	0.008
C8—C7—C6—C10			-0.1	-0.017	-0.289	Fe—C5—C1—C2			-60	-59.78	-60.066
C4—C5—C1—Fe			60.3	59.799	60.138	-			-	-	-

a : 6-311++ G(d, p) , b: LanL2DZ

3.1.2. N-ferrocenylméthyl-N-phenylpropionamide (FPP)

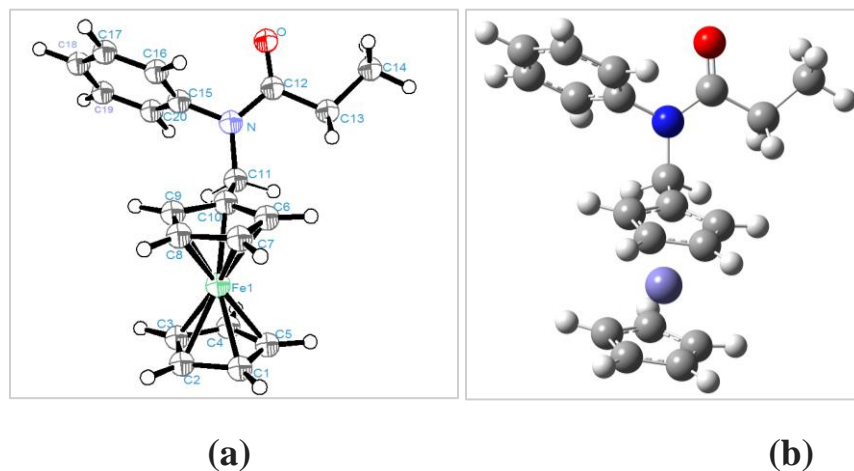**(a)**   **(b)**

Fig. 2. (a) The ORTEP view of FPP shows atomic labelling scheme and 40% probability level

dis-placement ellipsoids. **(b)** DFT optimized structure of FPP by GaussView

Table 2. Selected optimized and experimental geometry parameters of compound FPP by

DFT/B3LYP method

FPP		X-Ray	a	b			X-Ray	a	b
Bond distances(Å)									
C1	Fe	2.060	2.078	2.119	C18	H18	0.995	1.084	1.087
C2	Fe	2.064	2.076	2.120	C19	H19	1.018	1.084	1.088
C3	Fe	2.042	2.078	2.122	C10	C6	1.433	1.430	1.446
C4	Fe	2.035	2.080	2.121	C1	C5	1.405	1.426	1.443
C5	Fe	2.046	2.070	2.121	C1	C2	1.411	1.426	1.443
C6	Fe	2.056	2.071	2.113	C2	C3	1.425	1.426	1.443
C7	Fe	2.058	2.075	2.119	C3	C4	1.419	1.426	1.444
C8	Fe	2.055	2.077	2.118	C4	C5	1.410	1.426	1.443
C10	Fe	2.045	2.075	2.120	C6	C7	1.432	1.425	1.441
C1	H1	0.987	1.080	1.081	C6	C10	1.433	1.432	1.446
C2	H2	1.003	1.080	1.081	C7	C8	1.425	1.426	1.443
C3	H3	1.015	1.080	1.081	C8	C9	1.426	1.424	1.440
C4	H4	1.066	1.080	1.082	C9	C10	1.431	1.431	1.444
C5	H5	0.985	1.080	1.081	C10	C11	1.501	1.507	1.510
C6	H6	0.890	1.080	1.081	C12	C13	1.513	1.530	1.533
C7	H7	0.975	1.080	1.081	C13	C14	1.523	1.528	1.550
C8	H8	0.919	1.080	1.081	C15	C16	1.391	1.395	1.408
C9	H9	0.901	1.080	1.081	C15	C20	1.395	1.395	1.409
C11	H11b	0.891	1.092	1.098	C17	C18	1.392	1.395	1.409
C11	H11a	0.919	1.088	1.090	C17	C16	1.393	1.392	1.406
C20	H20	0.949	1.085	1.088	C19	C18	1.392	1.393	1.408
C13	H13a	0.970	1.094	1.097	C19	C20	1.392	1.394	1.407
C13	H13b	0.970	1.096	1.095	C20	C15	1.395	1.395	1.409

C14	H14b		0.959	1.091	1.097	C20	C19		1.392	1.394	1.407
C14	H14c		0.960	1.091	1.096	C11	N		1.486	1.479	1.493
C14	H14a		0.960	1.093	1.097	C12	O		1.229	1.220	1.260
C16	H16		0.915	1.083	1.085	C12	N		1.368	1.384	1.396
C17	H17		0.994	1.084	1.087	C15	N		1.439	1.439	1.451
						regression coefficients (R2)				**0.9816**	**0.9813**
Bond angles (°)											
H1	C1	C5	123.41	125.99	125.99	O	C12	N	121.49	121.38	121.42
H1	C1	C2	127.72	125.98	125.99	O	C12	C13	121.92	119.19	121.12
H1	C1	Fe	126.84	124.90	124.75	N	C12	C13	116.58	119.42	117.45
C5	C1	C2	108.86	108.02	108.01	H13a	C13	H13b	107.88	107.25	106.13
C5	C1	Fe	69.46	70.15	70.02	H13a	C13	C12	109.17	112.48	109.16
C2	C1	Fe	70.17	70.14	69.87	H13a	C13	C14	109.13	110.55	110.24
H2	C2	C1	127.49	126.00	125.92	H13b	C13	C12	109.17	104.78	108.84
H2	C2	C3	125.15	125.99	125.97	H13b	C13	C14	109.11	108.71	110.02
H2	C2	Fe	124.23	124.91	124.57	C12	C13	C14	112.28	112.70	112.25
C1	C2	C3	107.29	108.01	108.02	H14b	C14	H14c	109.52	108.13	107.28
C1	C2	Fe	69.83	70.06	69.98	H14b	C14	H14a	109.48	107.87	108.52
C3	C2	Fe	68.84	70.17	70.00	H14b	C14	C13	109.50	110.24	111.07
H3	C3	C4	127.16	126.05	126.02	H14c	C14	H14a	109.44	108.17	108.62
H3	C3	C2	125.00	125.96	126.00	H14c	C14	C13	109.46	110.23	111.12
H3	C3	Fe	123.45	125.36	124.89	H14a	C14	C13	109.43	112.09	110.13
C4	C3	C2	107.79	107.96	107.97	C16	C15	C20	120.33	119.83	119.66
C4	C3	Fe	69.36	70.08	69.99	C16	C15	N	119.47	120.69	120.74
C2	C3	Fe	70.53	70.07	69.85	C20	C15	N	120.17	119.48	119.56
H4	C4	C5	118.42	126.03	125.99	H16	C16	C15	118.05	119.50	119.40
H4	C4	C3	133.50	125.97	125.99	H16	C16	C17	122.51	120.59	120.61
H4	C4	Fe	122.74	125.87	125.37	C15	C16	C17	119.44	119.91	119.99
C5	C4	C3	108.00	108.00	108.02	H17	C17	C18	122.12	120.01	120.06
C5	C4	Fe	70.21	70.09	69.95	H17	C17	C16	117.35	119.56	119.60
C3	C4	Fe	69.89	70.14	69.89	C18	C17	C16	120.40	120.43	120.34
H5	C5	C1	122.95	125.92	125.97	H18	C18	C17	118.18	120.20	120.15
H5	C5	C4	128.96	126.10	126.05	H18	C18	C19	121.55	120.22	120.16
H5	C5	Fe	127.18	125.40	125.00	C17	C18	C19	119.97	119.58	119.69
C1	C5	C4	108.06	107.98	107.98	H19	C19	C18	118.26	120.15	120.20
C1	C5	Fe	70.52	70.05	69.87	H19	C19	C20	121.88	119.72	119.73
C4	C5	Fe	69.37	70.12	69.94	C18	C19	C20	119.85	120.12	120.06
H6	C6	C7	128.39	125.71	125.67	H20	C20	C19	122.14	119.93	120.23
H6	C6	C10	123.38	125.99	125.89	H20	C20	C15	117.82	119.93	119.54
H6	C6	Fe	127.90	125.63	124.25	C19	C20	C15	119.94	120.14	120.22
C7	C6	C10	108.21	108.30	108.41	C12	N	C15	122.82	119.38	118.54
C7	C6	Fe	69.71	70.32	70.05	C12	N	C11	119.50	124.30	124.66
C10	C6	Fe	69.16	70.28	69.96	C15	N	C11	117.46	116.32	116.64
H7	C7	C8	123.45	126.09	126.08	C4	Fe	C9	108.54	125.11	124.54
H7	C7	C6	128.57	125.96	125.99	C4	Fe	C3	40.75	39.79	40.12
H7	C7	Fe	124.38	125.11	124.59	C4	Fe	C10	110.10	109.90	109.08
C8	C7	C6	107.93	107.94	107.92	C4	Fe	C5	40.43	39.79	40.11
C8	C7	Fe	69.60	70.08	69.99	C4	Fe	C8	136.09	160.03	159.83
C6	C7	Fe	69.54	69.87	89.74	C4	Fe	C6	140.37	124.41	123.97
H8	C8	C7	127.91	126.06	126.00	C4	Fe	C7	176.61	159.12	159.01
H8	C8	C9	123.95	126.03	125.96	C4	Fe	C1	67.62	66.83	67.41
H8	C8	Fe	129.30	125.35	124.78	C4	Fe	C2	68.21	66.81	67.43
C7	C8	C9	108.04	107.91	108.03	C9	Fe	C3	112.22	109.52	108.59
C7	C8	Fe	69.85	70.11	69.84	C9	Fe	C10	41.00	39.87	40.37

C9	C8	Fe	69.14	70.01	69.75	C9	Fe	C5	134.58	160.58	160.48
H9	C9	C8	127.06	126.14	126.04	C9	Fe	C8	40.74	39.77	40.15
H9	C9	C10	124.41	125.44	125.55	C9	Fe	C6	68.55	66.85	67.61
H9	C9	Fe	124.42	125.99	125.13	C9	Fe	C7	68.49	66.79	67.57
C8	C9	C10	108.50	108.41	108.41	C9	Fe	C1	174.55	158.32	157.98
C8	C9	Fe	70.13	70.23	70.10	C9	Fe	C2	143.15	123.56	122.78
C10	C9	Fe	69.64	70.22	69.93	C3	Fe	C10	140.42	124.28	123.50
C9	C10	C6	107.32	107.44	107.24	C3	Fe	C5	68.11	66.81	67.43
C9	C10	C11	126.54	125.87	125.89	C3	Fe	C8	111.35	124.19	123.61
C9	C10	Fe	69.35	69.91	69.70	C3	Fe	C6	178.60	159.61	159.37
C6	C10	C11	126.15	126.70	126.83	C3	Fe	C7	138.21	159.29	159.07
C6	C10	Fe	69.93	69.78	69.63	C3	Fe	C1	67.68	66.81	67.45
C11	C10	Fe	125.69	125.67	127.48	C3	Fe	C2	40.63	39.77	40.15
H11b	C11	H11a	106.68	107.15	106.71	C10	Fe	C5	108.26	124.98	124.50
H11b	C11	N	105.45	109.11	107.33	C10	Fe	C8	68.88	67.00	67.80
H11b	C11	C10	112.80	109.16	109.55	C10	Fe	C6	40.91	39.94	40.41
H11a	C11	N	104.27	108.38	109.06	C10	Fe	C7	68.90	67.01	67.89
H11a	C11	C10	113.32	109.17	110.17	C10	Fe	C1	135.70	139.06	160.03
N	C11	C10	113.57	113.09	113.75	C10	Fe	C2	175.61	159.02	158.62
C5	Fe	C8	175.12	159.36	158.17	C8	Fe	C1	144.68	123.03	122.47
C5	Fe	C6	112.27	109.47	108.94	C8	Fe	C2	115.25	108.54	107.75
C5	Fe	C7	142.88	123.59	123.13	C6	Fe	C7	40.74	39.81	40.21
C5	Fe	C1	40.03	39.80	40.11	C6	Fe	C1	111.66	124.20	123.84
C5	Fe	C2	67.73	66.82	67.42	C6	Fe	C2	138.10	159.30	159.23
C8	Fe	C6	68.40	66.89	67.53	C7	Fe	C1	115.46	108.57	107.90
C8	Fe	C7	40.55	39.81	40.17	C7	Fe	C2	113.03	123.71	123.15
			40.01	39.80	40.15	**regression coefficients (R²)**				**0.9641**	**0.9665**
C1	Fe	C2									

Dihedral angles (°)

C15—N—C11—C10	-83.8	-78.538	-57.128	C7—C6—C10—Fe	-58.97	-59.723	-60.301
C11—N—C12—O	-0.7	-177.19	-175.29	C7—C6—C10—C9	0.6	0.099	0.26
C11—N—C12—C13	-179.74	-3.908	-4.916	C7—C6—C10—C11	-179.1	-178.081	-179.669
C15—N—C12—O	-175.3	-1.968	-4.918	Fe—C7—C8—C9	-58.77	-59.517	-60.066
C15—N—C12—C13	5.6	179.13	178.874	C6—C7—C8—Fe	59.16	59.666	59.862
C11—N—C15—C16	-101.1	-109.21	-120.5	C6—C7—C8—C9	0.4	0.149	0.204
C11—N—C15—C20	76.5	69.712	58.807	Fe—C8—C9—C10	-59.27	-59.661	-60.091
C12—N—C15—C16	73.6	66.391	59.692	C7—C8—C9—Fe	59.22	59.574	60.133
C12—N—C15—C20	-108.7	-114.68	-121	C7—C8—C9—C10	-0.1	-0.087	-0.042
Fe—C1—C2—C3	58.87	59.776	60.187	Fe—C9—C10—C6	-59.88	-59.773	-59.96
C5—C1—C2—Fe	-58.83	-59.804	-60.119	Fe—C9—C10—C11	119.8	122.221	120.11
C5—C1—C2—C3	0	0.029	0.069	C8—C9—C10—Fe	59.58	59.766	60.094
Fe—C1—C5—C4	-59.4	-59.76	-60.158	C8—C9—C10—C6	-0.3	-0.007	-0.134
C2—C1—C5—Fe	59.27	59.761	60.077	C8—C9—C10—C11	179.4	178.013	179.796
C2—C1—C5—C4	-0.2	-0.001	-0.082	Fe—C10—C11—N	173.98	171.501	171.692
Fe—C2—C3—C4	59.6	59.917	60.164	C6—C10—C11—N	-96	-96.998	-81.444
C1—C2—C3—Fe	-59.49	-59.872	-60.193	C9—C10—C11—N	84.5	80.622	98.472
C1—C2—C3—C4	0.1	0.046	0.029	O—C12—C13—C14	-10.3	-2.562	-92.003
Fe—C3—C4—C5	60.1	59.859	60.073	N—C12—C13—C14	168.8	178.533	88.201
C2—C3—C4—Fe	-60.34	-59.904	-60.095	N—C15—C16—C17	177.5	178.778	179.907
C2—C3—C4—C5	-0.2	-0.045	-0.021	C20—C15—C16-C17	-0.2	-0.15	-0.211
Fe—C4—C5—C1	60.16	59.797	60.132	N—C15—C20—C19	-176.1	-178.289	-178.71
C3—C4—C5—Fe	-59.93	-59.77	-60.068	C16—C15—C20-C19	1.5	0.648	0.606
C3—C4—C5—C1	0.2	0.027	0.064	C15—C16—C17-C18	-1.9	-0.402	-0.335
Fe—C6—C7—C8	-59.2	-5.825	-59.99	C16—C17—C18--C19	2.7	0.456	0.485
C10—C6—C7—Fe	58.61	59.671	60.277	C17—C18—C19-C20	-1.3	-0.042	-0.088
C10—C6—C7—C8	-0.6	-0.154	-0.288	C18—C19—C20-C15	-0.8	-0.594	-0.456

| Fe—C6—C10—C9 | 59.52 | 59.822 | 60.041 | Fe—C6—C10—C11 | -120.1 | -122.196 | -120.03 |

a : 6-311++ G(d,p) , b: LanL2DZ

3.1.3. N-ferrocenylmethyl-N-phenylbenzamide (FPB)
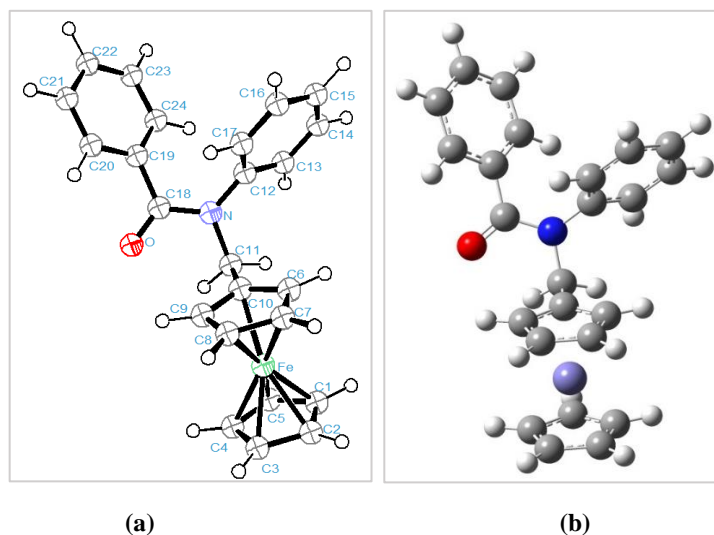

(a)   **(b)**

Fig. 3. (a) The ORTEP view of FPB shows the atomic labelling scheme and 40% probability level dis-placement ellipsoids. **(b)** DFT optimized structure of FPB by GaussView

Table 3. Selected optimized and experimental geometry parameters of compound FPB by DFT/B3LYP method

FPB		X-ray	a	b			X-ray	a	b
Bond distances(Å)									
Fe	C1	2.056	2.07786	2.1208	C9	C10	1.425	1.43099	1.44489
Fe	C2	2.04	2.07784	2.11979	C14	C15	1.385	1.3948	1.40923
Fe	C3	2.044	2.07663	2.11863	C15	C16	1.388	1.39336	1.40823
Fe	C4	2.052	2.07709	2.12036	C16	C17	1.39	1.39317	1.40621
Fe	C5	2.063	2.07699	2.12061	C18	C19	1.51	1.50529	1.50542
Fe	C6	2.038	2.07273	2.11362	C19	C20	1.389	1.39953	1.41238
Fe	C7	2.031	2.07538	2.11583	C19	C24	1.393	1.39875	1.41224
Fe	C8	2.037	2.07651	2.11786	C20	C21	1.385	1.39137	1.40479
Fe	C9	2.039	2.07424	2.11712	C21	C22	1.375	1.39479	1.40908
Fe	C10	2.05	2.07222	2.11779	C22	C23	1.388	1.39387	1.40841
C1	C2	1.41	1.42607	1.44315	C23	C24	1.383	1.39297	1.40596
C1	C5	1.423	1.42655	1.44374	C10	C11	1.501	1.5038	1.50733
C2	C3	1.42	1.42623	1.44336	C12	C13	1.389	1.3987	1.41103
C3	C4	1.418	1.42605	1.44311	C12	C17	1.395	1.39674	1.40978
C4	C5	1.411	1.42606	1.44315	C13	C14	1.392	1.39213	1.40583
C6	C7	1.428	1.42484	1.4416	O	C18	1.224	1.22547	1.26507
C6	C10	1.433	1.43133	1.44564	N	C11	1.482	1.48545	1.4996
C7	C8	1.429	1.42679	1.44429	N	C12	1.438	1.43222	1.44276

C8		C9	1.428	1.42421	1.44052	N		C18	1.371	1.38275	1.39449
						regression coefficients (R2)				**0.9993**	**0.9986**
Bond angles (°)											
C1	Fe	C2	40.28	40.139	39.793	Fe	C2	C3	69.8	69.876	70.047
C4	Fe	C9	110.68	108.137	108.895	C1	C2	C3	108.3	108	107.994
C1	Fe	C3	60.07	67.482	66.846	Fe	C3	C2	69.5	69.968	70.134
C4	Fe	C10	117.8	123.245	123.936	Fe	C3	C4	70	69.938	70.161
C1	Fe	C4	57.78	67.503	66.839	C2	C3	C4	107.5	108.037	108.032
C5	Fe	C6	115.94	123.985	124.536	Fe	C4	C3	69.5	69.903	70.032
C1	Fe	C5	40.41	40.162	39.802	Fe	C4	C5	70.4	69.919	70.115
C5	Fe	C7	147.54	159.477	159.622	C3	C4	C5	108.4	108.037	107.974
C1	Fe	C6	106.91	108.988	109.72	Fe	C5	C1	69.5	69.952	70.106
C5	Fe	C8	170.78	159.066	159.292	Fe	C5	C4	69.5	69.926	70.096
C1	Fe	C7	114.38	123.741	124.478	C1	C5	C4	107.9	108.045	108.022
C5	Fe	C9	131.85	123.691	124.338	Fe	C6	C7	69.2	70.01	70.154
C1	Fe	C8	147.63	159.061	159.129	Fe	C6	C10	69.93	69.78	70.179
C5	Fe	C10	109.04	108.529	109.521	C7	C6	C10	108.4	108.304	108.213
C1	Fe	C9	169.52	159.637	159.957	Fe	C7	C6	69.7	69.81	69.989
C6	Fe	C7	41.1	40.179	39.857	Fe	C7	C8	69.7	69.943	70.129
C1	Fe	C10	129.87	123.947	124.737	C6	C7	C8	107.8	107.912	107.878
C6	Fe	C8	68.99	67.518	66.916	Fe	C8	C7	69.2	69.858	69.978
C2	Fe	C3	40.7	40.159	39.82	Fe	C8	C9	69.6	69.847	70.087
C6	Fe	C9	68.77	67.623	66.952	C7	C8	C9	107.9	108.106	108.068
C2	Fe	C4	68.03	67.491	66.85	Fe	C9	C8	69.4	70.018	70.142
C6	Fe	C10	41.04	40.403	39.954	Fe	C9	C10	70	69.735	70.076
C2	Fe	C5	67.86	67.446	66.831	C8	C9	C10	108.6	108.223	108.168
C7	Fe	C8	41.12	40.199	39.893	Fe	C10	C6	69.03	69.818	69.867
C2	Fe	C6	128.58	123.927	124.452	Fe	C10	C9	69.18	69.887	70.026
C7	Fe	C9	69.13	67.588	66.953	Fe	C10	C11	127.5	126.851	125.647
C2	Fe	C7	106.59	108.466	109.032	C6	C10	C9	107.3	107.453	107.673
C7	Fe	C10	69.32	67.861	67.074	C11	N	C12	118.6	116.978	116.912
C2	Fe	C8	115.92	123.237	123.601	C11	N	C18	118.4	116.886	116.638
C8	Fe	C9	41.02	40.134	39.772	C12	N	C18	122.7	124.285	124.736
C2	Fe	C9	149.77	158.589	158.646	C13	C12	C17	120.5	119.4	119.645
C8	Fe	C10	69.07	67.775	66.968	C12	C14	C14	119.4	120.271	120.148
C2	Fe	C10	167.82	159.297	160.02	C13	C14	C15	120.5	120.209	120.225
C9	Fe	C10	40.79	40.377	39.898	C14	C15	C16	119.6	119.599	119.566
C3	Fe	C4	40.5	40.158	39.807	C15	C17	C17	120.7	120.346	120.364
C3	Fe	C5	67.91	67.471	66.833	C12	C17	C16	119.1	120.161	120.039
C3	Fe	C6	167.97	159.283	159.459	O	C18	N	121.8	121.246	120.383
C3	Fe	C7	129.74	123.359	123.788	O	C18	C19	121.2	119.642	119.673
C3	Fe	C8	108.98	108.021	108.587	N	C18	C19	117	119.064	119.9
C3	Fe	C9	118.04	122.962	123.417	C18	C19	C20	118.5	117.316	117.229
C3	Fe	C10	150.39	158.702	158.87	C18	C19	C24	122.1	123.238	123.267
C4	Fe	C5	40.1	40.155	39.789	C29	C19	C24	119.3	119.228	119.318
C4	Fe	C6	149.2	159.352	159.544	C19	C20	C21	119.9	120.44	120.445
C4	Fe	C7	169.58	158.896	159.056	C20	C21	C22	120.8	120.051	120.028
C4	Fe	C8	132.05	123.213	123.713	C21	C22	C23	119.5	119.789	119.745
Fe	C1	C2	69.2	69.93	70.066	C22	C23	C24	120.3	120.207	120.257
Fe	C1	C5	70.1	69.886	70.092	C19	C24	C23	120.2	120.255	120.185
C2	C1	C5	107.9	107.962	107.978	C6	C10	C11	126.3	126.38	126.441
Fe	C2	C1	70.5	69.931	70.141	C9	C10	C11	126.4	126.147	125.886
N	C11	C10	113	113.376	112.957	N	C12	C17	119.8	120.938	120.708

N	C12	C13	119.7	119.623	119.598	regression coefficients (R2)		0.9855	0.9855
Dihedral angles (°)									
C12—N—C11—C10		-	75.299	76.349	C7—C6—C10—C11	-	178.845	179.841	
C11—N—C18—O		-	3.555	4.999	Fe—C7—C8—C9	-	59.601	59.987	
C11—N—C12—C13		-	66.136	63.98	C6—C7—C8—Fe	-	59.726	60.072	
C12—N—C18—O		-	160.443	159.574	C6—C7—C8—C9	-	0.125	0.085	
C12—N—C18—C19		-	22.048	22.844	Fe—C8—C9—C10	-	59.489	60.01	
C11—N—C12—C17		-	111.556	113.491	C7—C8—C9—Fe	-	59.608	59.919	
C18—N—C12—C13		-	129.879	131.486	C7—C8—C9—C10	-	0.12	0.091	
C18—N—C12—C17		-	52.428	51.044	Fe—C9—C10—C6	-	59.981	59.989	
Fe—C1—C2—C3		-	59.745	60.079	Fe—C9—C10—C11	-	121.563	120.159	
C5—C1—C2—Fe		-	59.78	60.1	C8—C9—C10—Fe	-	59.665	60.051	
C5—C1—C2—C3		-	0.035	0.021	C8—C9—C10—C6	-	0.316	0.062	
Fe—C1—C5—C4		-	59.791	60.102	C8—C9—C10—C11	-	178.772	179.79	
C2—C1—C5—Fe		-	59.807	60.084	Fe—C10—C11—N	-	174.178	173.64	
C2—C1—C5—C4		-	0.016	0.018	C6—C10—C11—N	-	94.869	96.187	
Fe—C2—C3—C4		-	59.82	60.191	C9—C10—C11—N	-	80.301	83.638	
C1—C2—C3—Fe		-	59.78	60.139	O—C18—C19—C24	-	137.021	141.966	
C1—C2—C3—C4		-	0.04	0.052	N—C12—C13—C14	-	178.266	178.004	
Fe—C3—C4—C5		-	59.808	60.11	N—C18—C19—C24	-	40.529	35.633	
C2—C3—C4—Fe		-	59.838	60.173	C17—C12—C13-C14	-	0.538	0.506	
C2—C3—C4—C5		-	0.03	0.063	N—C18—C19—C20	-	144.878	149.371	
Fe—C4—C5—C1		-	59.807	60.108	C13—C12—C17-C16	-	1.339	1.25	
C3—C4—C5—Fe		-	59.798	60.058	C12—C13—C14-C15	-	0.405	0.38	
C3—C4—C5—C1		-	0.009	0.05	C13—C14—C15-C16	-	0.547	0.521	
Fe—C6—C7—C8		-	59.81	60.161	C14—C15—C16-C17	-	0.258	0.226	
C10—C6—C7—Fe		-	59488	60.114	C15—C16—C17-C12	-	1.207	1.115	
C10—C6—C7—C8		-	0.322	0.047	O—C18—C19—C20	-	37.572	33.03	
Fe—C6—C10—C9		-	60.026	60.089	C19—C20—C21-C22	-	1.525	1.17	
Fe—C6—C10—C11		-	121.524	120.06	C20—C21—C22-C23	-	0.095	0.136	
C7—C6—C10—Fe		-	59.632	60.099	C21—C22—C23-C24	-	1.109	0.963	
C7—C6—C10—C9		-	0.394	0.01	C22—C23—C24-C19	-	0.891	0.488	

a : 6-311++ G(d, p) , b: LanL2DZ

3.2. Atomic charges

The Mulliken charge plays an essential role in determining the atoms' vibrational properties. Additionally, they demonstrate atoms with negative charges and atoms with positive charges. Indeed, it figures out which atom is electron donor and which one is electron acceptor. So, it can determine the dipole moment and polarizability of the molecule [22]. In this study, Mulliken atomic charges between constituent atoms of FPA, FPP and FPB were calculated using the computational methods DFT/ B3LYP with 6-311++G (d, p) and LanL2DZ basis sets. Results are shown in figure 4 and both bases were compared with each other. According to Mulliken population in the figure 4, it can be seen in both basis set that most of carbon and oxygen atoms have negative charges, for nitrogen and iron atoms show positive charges using 6-311++G (d,p) basis set and negative charges using LanL2DZ basis set, however, the MESP maps (figure 5) shows coincidence with the 6-

311++g(d,p) basis set. Thus, negative charge leads to electrophilic substitution, while positive charge leads to preferential site to nucleophilic attack.
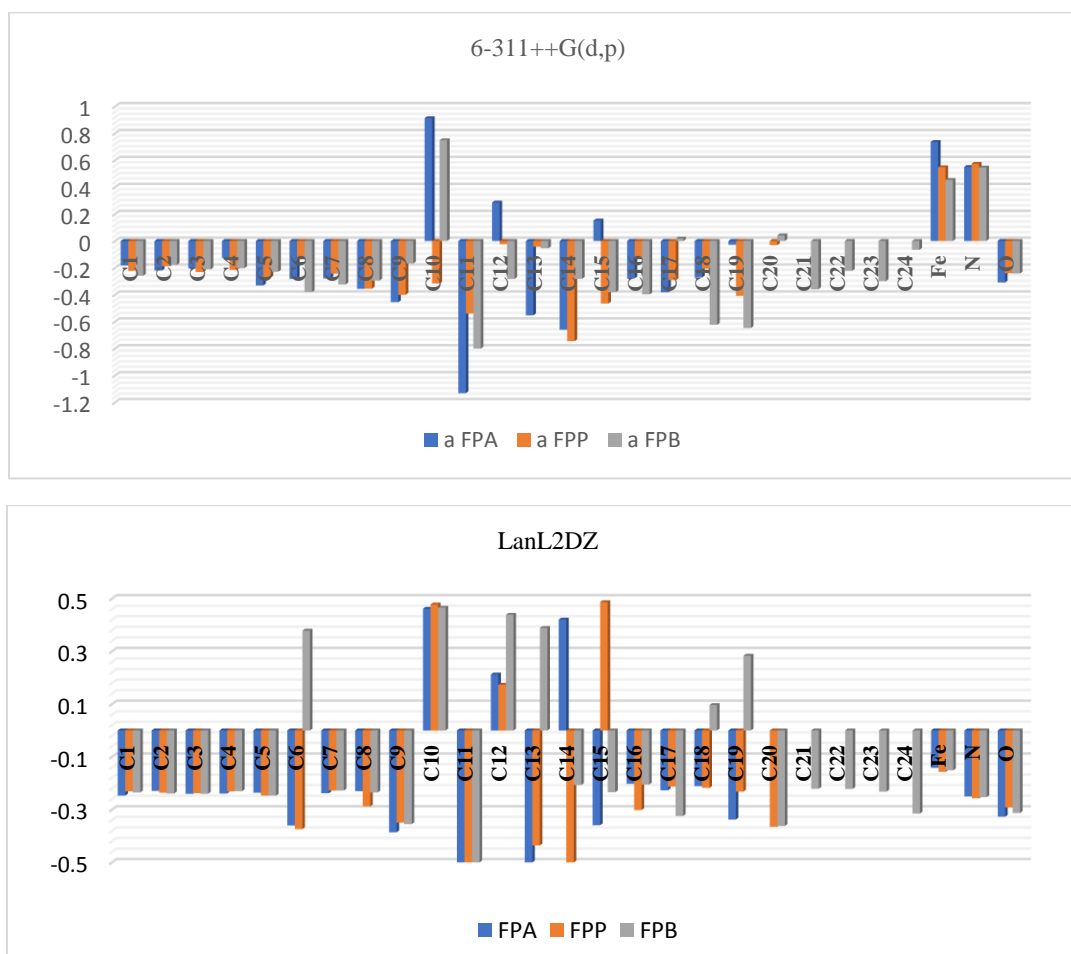
Fig. 4. Muliken atomic charges for FPA, FPP and FPB by DFT/B3LYP method with 6-311++ G (d,p) and LanL2DZ basis sets

3.3. Molecular electrostatic potential map (MESP)

MESP is an important factor which is employed to predict reactive sites for electrophilic and nucleophilic attack. MESP surface concurrently shows molecular size, shape and electrostatic potential using color grading and it is very helpful means to prove the correlation between chemical structure and the physicochemical properties of biomolecules [23-26]. For the color coding, the blue corresponds to extremely electron deficient regions and the red corresponds to electron rich

regions, whereas the green regions signify electrically neutral regions. Potential decreases in this order: red < orange < yellow < green < blue.

MESP maps of the three studied molecules have been determined by B3LYP/6-311++ G (d, p) method. As it's shown in figure 5 the most electron rich regions (red and orange) are located around oxygen atoms, which reflect the most electronegative regions, there is also others electron rich regions (yellow) in the middle of cyclopentadienyls of the ferrocene and benzene rings which refer to the existence of carbon atoms that have negative charges as it's mentioned in figure 4.

(a)   (b)   (c)
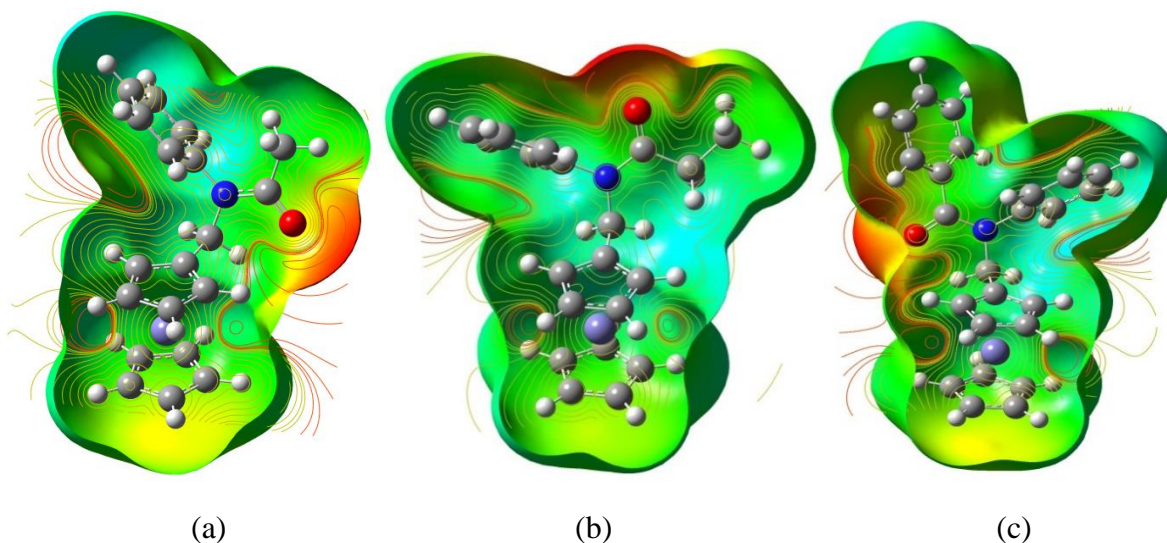
Fig. 5. MESP Surface and contour map for (a): FPA (b): FPP and (c): FPB

3.4. NMR Spectrum Analysis

The optimized structures of the three studied compounds were used to calculate the ^{1}H and ^{13}C NMR spectra using Gaussian 09 software, DFT/B3LYP and the gauge independent atomic orbital (GIAO) methods with 6-31++G(d,p) and LanL2DZ basis set and Chloroform as solvent. The chemical shifts of the compounds FPA, FPP and FPB were computed with reference to TMS B3LYP / 6-311 ++G (d, p) GIAO. The obtained values were compared to each other and then to the experimental chemical shifts [27].

Looking at table 4 which shows ^{1}H NMR results, it is apparent that the experimental chemical shifts of the ferrocenic part of the three molecules are around 4.00 ppm, whereas, the chemical shifts of both computational basis 6-311++G(d,p)and LanL2DZ are between 2.61 and 4.51 ppm where the chemical shifts obtained from LanL2dz basis set are lower. On the other hand, the chemical shifts for the rest of FPA, FPP and FPB are in the range of 5.94 to 7.71 ppm in

experimental and both computational bases, except for methyl group of FPA and ethyl group of FPP are very close to the TMS reference line with values near to 1.00 ppm.

It is clear from the results that the calculated chemical shifts using Gaussian 09 software and experimental ones for ^{1}H NMR are very close to each other, where the values of 6-311++G (d, p) are closer.

Table 5 compares the calculated and the experimental ^{13}C NMR results of the three studied compounds. It can be seen that the chemical shifts of ferrocenic part's carbon are all near to each other where the experimental chemical shifts are in the range of 68.55 - 83.33 ppm. Furthermore, the chemical shifts obtained from 6-311++ G(d,p) basis set are in the range of 90.35 - 70.03ppm, whereas, the LanL2DZ basis set has given smaller chemical shifts in the range of 81.98 and 58.70ppm. The aromatic carbon atoms generally give rise to signals in the range of 100–150 ppm [20], the aromatic carbons of FPA, FPP and FPB also observed in the expected range from 118.82 to 149.43 ppm. The carbonyl groups are highly deshielded between 178.18 and 169.16 ppm and the least chemical shifts are for methyl and ethyl groups of FPA and FPP respectively from 7.18 to 26.39 ppm.

Table 4. Calculated ^{1}H NMR chemical shift (ppm) of FPA, FPP and FPB CDCl$_3$ by experimental method and DFT/B3LYP methods

FPA				FPP				FPB			
Atom	Exp	a	b	Atom	Exp	a	b	Atom	Exp	a	b
H6	4.03	3.18	2.61	H6	4.04	3.02	2.66	H6	4.18	4.51	4.14
H9	4.03	4.21	3.80	H9	4.04	3.79	3.32	H7	4.10	3.76	3.24
H7	4.03	3.59	3.06	H8	4.04	3.79	3.21	H8	4.10	3.51	2.99
H8	4.03	3.70	3.27	H7	4.04	3.65	2.90	H9	4.18	3.13	2.61
H5	4.08	3.59	3.13	H5	4.08	3.65	3.21	H1	4.16	3.64	3.09
H1	4.08	3.59	3.06	H1	4.08	3.56	2.99	H2	4.16	3.76	3.24
H2	4.08	3.88	3.50	H2	4.08	3.79	3.32	H3	4.16	3.76	3.24
H3	4.08	3.59	3.36	H3	4.08	3.79	3.32	H4	4.16	3.76	3.38
H4	4.08	3.59	3.27	H4	4.08	3.65	3.32	H5	4.16	3.93	3.48
H11	4.61	5.86	2.66	H11	4.61	4.79	4.19	H11	4.89	4.14	5.07
H19	6.97	6.61	5.94	H20	6.97	7.44	6.74	H17	6.93	6.25	5.56
H18	7.28	7.28	6.88	H19	7.30	7.68	7.011	H16	7.13	7.02	6.56
H17	7.30	7.55	7.12	H18	7.33	7.44	6.85	H15	7.16	7.31	6.92
H16	7.32	7.70	7.23	H17	7.35	7.44	6.74	H14	7.18	7.71	7.20
H15	7.26	7.39	6.88	H16	7.29	6.76	6.46	H13	6.91	7.71	7.11
H13	1.75	1.62	0.85	H13	1.96	2.50	1.96	H20	7.26	7.97	7.50
-	-	-	-	H14	1.02	1.10	0.84	H21	7.13	7.51	7.01
-	-	-	-	-	-	-	-	H22	7.16	7.51	7.01
-	-	-	-	-	-	-	-	H23	7.18	7.02	6.56
-	-	-	-	-	-	-	-	H24	7.29	7.02	6.27

a : 6-311++ G(d, p) , b: LanL2DZ

Table 5. Calculated ^{13}C NMR chemical shift (ppm) of FPA, FPP and FPB in CDCl$_3$ by experimental method and DFT/B3LYP methods

FPA				FPP				FPB			
Atom	Exp	a	b	Atom	Exp	a	b	Atom	Exp	a	b
C1	68.55	73.32	62.11	C1	68.57	73.35	61.88	C1	68.69	72.07	59.85
C2	68.55	72.20	60.52	C2	68.57	72.754	59.93	C2	68.69	71.58	59.93
C3	68.55	70.99	59.91	C3	68.57	72.52	60.16	C3	68.69	71.15	60.11
C4	68.55	70.53	59.81	C4	68.57	72.44	60.16	C4	68.69	70.97	60.28
C5	68.55	71.20	59.98	C5	68.57	71.81	60.22	C5	68.69	73.01	61.88
C6	77.16	75.04	64.86	C6	77.16	72.52	63.49	C6	77.16	73.89	63.95
C7	77.58	72.55	61.61	C7	77.59	71.46	61.24	C8	77.58	71.85	60.87
C8	77.58	70.03	58.70	C8	77.59	72.75	59.70	C7	77.58	70.89	58.95
C9	77.16	73.65	64.81	C9	77.16	74.46	65.14	C9	77.16	75.96	66.47
C10	83.33	90.35	81.98	C10	83.33	89.186	80.44	C10	83.26	88.78	80.58
C11	48.40	51.05	45.11	C11	48.65	53.10	46.51	C11	49.88	53.59	48.29
C12	169.74	172.95	169.16	C12	173.17	178.18	174.41	C12	126.75	151.68	138.54
C13	22.83	23.40	17.35	C13	27.87	31.16	26.39	C13	128.33	132.72	121.56
C14	127.87	151.99	137.31	C14	9.67	8.78	7.18	C14	128.97	134.03	122.95
C15	128.55	133.80	122.75	C15	127.86	149.43	134.40	C15	128.97	130.91	119.89
C16	129.43	134.32	123.74	C16	128.77	137.83	125.85	C16	128.97	133.38	122.52
C17	129.43	132.41	121.89	C17	129.46	132.61	121.01	C17	128.33	136.16	124.71
C18	129.43	133.30	122.75	C18	129.46	131.29	119.39	C18	170.07	176.85	171.19
C19	128.55	136.98	125.62	C19	129.46	134.26	121.56	C19	127.68	142.50	127.18
-	-	-	-	C20	128.77	132.22	118.82	C20	128.77	136.49	126.50
-	-	-	-	-	-	-	-	C21	129.50	132.78	121.65
-	-	-	-	-	-	-	-	C22	129.50	134.99	123.33
-	-	-	-	-	-	-	-	C23	129.50	131.02	119.89
-	-	-	-	-	-	-	-	C24	128.77	134.53	123.71

a : 6-311++ G(d, p) , b: LanL2DZ

3.5. Vibrational analysis

The studied molecules FPA, FPP and FPB have 117, 126 and 138 vibration modes, respectively. All those vibrational modes are active in IR (figure 6). The most important stretching and bending vibrations along with their probable assignments of the title molecules are given in Tables 6, 7 and 8. All of these vibrations were measured by the computational methods of DFT / B3LYP with 6-311 ++ G(d,p) and LanL2DZ basis sets. Also, the experimental FT IR spectra was measured in order to better identifying the compounds and the amount of computational frequencies were compared to experimental frequencies.

The experimental infrared spectra of FPA, FPP and FPB are shown in Fig. 7.

It can be seen from the results that the simulated frequencies by Gaussian 09 software were higher than experimental frequencies. So, these frequencies should be multiplied by Scalling factor to be close to the experimental frequencies.

Table 6. The observed FT-IR of FPA and its calculated wavenumbers (in cm^{-1}) with their probable assignments

Experimental frequencies (cm-1)	Calculated frequencies				Vibrational Assignments
	6-311++G(d,p)		Lan2dz		
FT-IR	unscaled	scaled	unscaled	Scaled	
2360	3243	3100	3302	3110	υ_w (C$_1$H$_1$C$_2$H$_2$C$_3$H$_3$C$_4$H$_4$C$_5$H$_5$)sy
	3240	3097	3296	3104	υ_m (C$_6$H$_6$C$_7$H$_7$C$_8$H$_8$C$_9$H$_9$)sy
	3232	3089	3283	3092	υ_w (C$_1$H$_1$C$_2$H$_2$C$_3$H$_3$C$_4$H$_4$C$_5$H$_5$C$_6$H$_6$C$_7$H$_7$)asy
	3194	3053	3233	3045	υ_w (C$_{15}$H$_{15}$C$_{16}$H$_{16}$C$_{17}$H$_{17}$C$_{18}$H$_{18}$C$_{19}$H$_{19}$)sy
	3180	3040	3212	3025	υ_w (C$_{15}$H$_{15}$C$_{16}$H$_{16}$C$_{17}$H$_{17}$C$_{18}$H$_{18}$C$_{19}$H$_{19}$)asy
	3147	3008	3147	2964	υ_w (C$_{13}$H$_{13a}$H$_{13b}$H$_{13c}$)asy
	3128	2990	3156	2972	υ_w (C$_{11}$H$_{11a}$H$_{11b}$)asy
	3062	2927	3088	2908	υ_w (C$_{11}$H$_{11a}$H$_{11b}$)sy
1651	1713	1637	1626	1531	υ_s(C$_{12}$O)sy
1593	1635	1563	1525	1436	υ_s(C$_{15}$C$_{16}$ C$_{18}$C$_{19}$)sy
	1497	1431	1510	1422	υ_m(C$_6$C$_{10}$ C$_9$)sy
1494	1486	1420	1509	1421	π_m (C$_{13}$H$_{13a}$H$_{13b}$H$_{13c}$)sy
	1473	1408	1504	1416	π_m (C$_{11}$H$_{11a}$H$_{11b}$)sy
1387	1371	1310	1416	1333	υ_m(C$_6$C$_{10}$ C$_9$ C$_1$C$_5$ C$_4$)asy+ υ_m (C$_{12}$N) sy
1284	1294	1237	1306	1230	υ_s (C$_{12}$C$_{11}$N) asy+α_s (C$_{11}$H$_{11a}$)asy
	1211	1157	1225	1153	α_m (C$_{11}$H$_{11a}$H$_{11b}$)asy+ υ_m(C$_6$C$_{10}$C$_9$)asy
1023	1133	1083	1122	1056	υ_w(C$_1$C$_2$ C$_3$ C$_4$C$_5$)sy
	1043	997	1048	987	υ_m(C$_6$C$_7$ C$_8$ C$_4$C$_9$)asy
806	841	803	815	767	α_m (C$_1$H$_1$C$_2$H$_2$C$_3$H$_3$C$_4$H$_4$C$_5$H$_5$C$_6$H$_6$C$_7$H$_7$C$_8$H$_8$)asy
701	731	698	726	683	α_m (C$_1$H$_1$C$_2$H$_2$C$_3$H$_3$C$_4$H$_4$C$_5$H$_5$C$_6$H$_6$C$_7$H$_7$C$_8$H$_8$)asy
561	506	483	494	465	υ_m (C$_6$FeC$_9$FeC$_4$FeC$_5$FeC$_{10}$FeC$_1$Fe)sy
544	479	457	459	432	υ_m(C$_6$FeC$_7$FeC$_8$FeC$_9$FeC$_2$FeC$_3$FeC$_4$FeC$_5$Fe)sy
	461	440	440	414	υ_m(C$_6$FeC$_7$FeC$_8$FeC$_9$FeC$_1$FeC$_2$FeC$_3$FeC$_4$FeC$_5$FeC$_{10}$Fe)asy

asy – asymmetric, Sy – symmetric, υ – stretching, π- in plane bending, α- out of plane bending, s - strong, m - medium.
Scaling factor (6-311g++dp = 0.956 , lanl2dz=0.942)

Table 7. The observed FT-IR of FPP and its calculated wavenumbers (in cm^{-1}) with their probable assignments

Experimental frequency (cm-1)	Calculated frequencies				Vibrational Assignments
	6-311++G(d,p)		Lan2dz		
FT-IR	unscaled	scaled	unscaled	scaled	
2159	3232	2954	3282	2976	$\upsilon_w(C_1H_1C_2H_2C_3H_3C_4H_4C_5H_5)asy$
	3230	2952	3281	2975	$\upsilon_w (C_6H_6C_7H_7 C_8H_8C_9H_9)asy$
	3178	2904	3226	2925	$\upsilon_m(C_{16}H_{16}C_{17}H_{17} C_{18}H_{18}C_{19}H_{19}C_{20}H_{20})asy$
	3127	2858	3181	2885	$\upsilon_w(C_{11}H_{11a}H_{11b})asy$
	3104	2837	3153	2859	$\upsilon_m(C_{13}H_{13a}H_{13b}C_{14}H_{14a}H_{14b}H_{14c})asy$
	3063	2799	3062	2777	$\upsilon_w (C_{11}H_{11a}H_{11b})sy$
	3040	2778	3049	2765	$\upsilon_m(C_{14}H_{14a}H_{14b}H_{14c})sy$
	3022	2762	3078	2791	$\upsilon_m(C_{13}H_{13a}H_{13b})sy$
1654	1722	1573	1618	1467	$\upsilon_s(C_{18}O)sy$
1592	1633	1492	1653	1499	$\upsilon_w(C_{16}C_{17} C_{18}C_{19})sy$
	1525	1393	1636	1483	$\upsilon_m(C_{15} C_{16} C_{17}C_{18} C_{19}C_{20})asy$
1493	1501	1371	1539	1395	$\pi_w(C_{14}H_{14a}H_{14b}H_{14c})sy+ \pi_w(C_{13}H_{13a}H_{13b})sy$
1469	1438	1314	1402	1271	$\upsilon_m(C_6 C_7 C_8C_9)asy$
1432	1418	1296	1415	1283	$\upsilon_m (C_{12}NC_{15}) asy+ \alpha_m(C_{13}H_{13a}H_{13b})asy+ \alpha_m(C_{11}H_{11a}H_{11b})sy$
1402	1393	1273	1388	1258	$\upsilon_m(C_1C_5 C_4)asy+ \upsilon_m(C_6C_{10} C_9)asy$
1374	1341	1225	1377	1248	$\alpha_m(C_{11}H_{11a}H_{11b})asy+ \alpha_m(C_{13}H_{13a}H_{13b})sy+ \upsilon_m (C_{12}NC_{15}) asy$
1262	1271	1161	1281	1161	$\alpha_m(C_{11}H_{11a}H_{11b})asy+ \pi_m (C_6H_6C_7H_7C_8H_8C_9H_9)sy$
	1256	1147	1270	1151	$\upsilon_m(C_6C_7 C_8 C_4C_9 C_{10}) sy$
	1235	1128	1245	1129	$\upsilon_m (C_{12}NC_{15}) asy++ \pi_m (C_{16}H_{16}C_{17}H_{17}C_{19}H_{19}C_{20}H_{20})asy$
1177	1194	1091	1214	1101	$\pi_m (C_{16}H_{16}C_{17}H_{17}C_{19}H_{19}C_{20}H_{20})asy$
1106	1133	1035	1122	1017	$\upsilon_m(C_1C_2 C_3 C_4C_5)sy$
1071	1125	1028	1134	1028	$\upsilon_m (C_{11}N) sy$
1023	1047	956	1056	957	$\pi_m (C_6H_6C_7H_7C_8H_8C_9H_9)asy$
925	847	744	810	734	$\alpha_m(C_1H_1C_2H_2C_3H_3C_4H_4C_5H_5C_6H_6C_7H_7C_8H_8C_9H_9C_{16}H_{16}C_{17}H_{17}C_{18}H_{18}C_{19}H_{19}C_{20}H_{20})asy$
806	836	764	791	717	$\alpha_m(C_1H_1C_2H_2C_3H_3C_4H_4C_5H_5)asy$

701	707	646	720		653	$\alpha_m(C_{16}H_{16}C_{17}H_{17}\ C_{18}H_{18}C_{19}H_{19}C_{20}H_{20})$asy
613	488	446	474		429	$\upsilon_m\ (C_{10}FeC_6FeC_9FeC_1FeC_4Fe)$sy
564	479	437	455		412	$\upsilon_m(C_1FeC_2FeC_3FeC_4FeC_5FeC_6Fe\ C_7FeC_8FeC_9Fe)$sy
	460	420	440		399	$\upsilon_m\ (C_1FeC_2FeC_3FeC_4FeC_5FeC_6Fe\ C_7FeC_8FeC_9Fe)$sy

asy – asymmetric, Sy – symmetric, υ – stretching, π- in plane bending, α- out of plane bending, s - strong, m - medium.
Scaling factor (6-311g++dp =0.914, lanl2dz= 0.907).

Table 8. The observed FT-IR of FPB and its calculated wavenumbers (in cm^{-1}) with their

probable assignments

Experimental frequency (cm-1)	Calculated frequencies				Vibrational Assignments
	6-311++G(d,p)		Lan2dz		
FT-IR	unscaled	scaled	unscaled	scaled	
2159	3233	2964	3285	2992	$\upsilon_w\ (C_6H_6C_7H_7\ C_8H_8C_9H_9)$asy
	3230	2961	3280	2988	$\upsilon_w(C_1H_1C_2H_2C_3H_3C_4H_4C_5H_5)$asy
	3222	2954	3271	2979	$\upsilon_w\ (C_6H_6C_7H_7C_8H_8C_9H_9)$asy
	3200	2934	3241	2952	$\upsilon_w\ (C_{20}H_{20}C_{21}H_{21}C_{22}H_{22}C_{23}H_{23}C_{24}H_{24})$sy
	3197	2931	3235	2947	$\upsilon_w\ (C_{13}H_{13}C_{14}H_{14}C_{15}H_{15}C_{16}H_{16}C_{17}H_{17})$sy
	3189	2924	3228	2940	$\upsilon_m\ (C_{13}H_{13}C_{14}H_{14}C_{15}H_{15}C_{16}H_{16}C_{17}H_{17})$asy
	3184	2919	3220	2933	$\upsilon_m(C_{20}H_{20}C_{21}H_{21}C_{22}H_{22}C_{23}H_{23}C_{24}H_{24})$asy
	3073	2817	3101	2825	$\upsilon_w\ (C_{11}H_{11a}H_{11b})$sy
1639	1690	1549	1584	1443	$\upsilon_s(C_{18}O)$sy
1594	1639	1502	1651	1504	$\upsilon_w(C_{20}C_{21}\ C_{23}C_{24})$sy
	1617	1482	1633	1487	$\upsilon_m(C_{19}C_{20}C_{21}\ C_{22}\ C_{23}C_{24})$asy
	1525	1398	1525	1389	$\upsilon_m(C_{12}C_{13}C_{14}\ C_{15}\ C_{16}C_{17})$asy+ $\upsilon_m\ (C_{12}NC_{18})$ asy
1490	1469	1347	1501	1367	$\pi_m\ (C_{11}H_{11a}H_{11b})$sy
1443	1406	1289	1437	1309	$\upsilon_m(C_6C_7\ C_8\ C_4C_9\ C_{10})$asy+ $\alpha_m\ (C_{11}H_{11a}H_{11b})$sy
1428	1385	1270	1412	1286	$\upsilon_m(C_1C_5\ \ C_4)$asy+ $\alpha_m\ (C_{11}H_{11a}H_{11b})$sy+ $\upsilon_m\ (C_{18}NC_{19})$ asy
1379	1371	1257	1391	1267	$\upsilon_m\ (C_{12}C_{18}N)$ asy+ $\upsilon_m(C_6C_{10}\ C_9)$asy
1369	1321	1211	1373	1250	$\upsilon_m(C_{12}C_{13}C_{14}\ C_{15}\ C_{16}C_{17})$asy
1295	1296	1188	1306	1189	$\upsilon_s(C_{19}C_{18}N)$ asy+ $\alpha_s(C_{11}H_{11a})$asy

1281	1270	1164	1284	1169	π_m (C$_6$H$_6$C$_7$H$_7$C$_8$H$_8$C$_9$H$_9$)sy+ α_m(C$_{11}$H$_{11a}$H$_{11b}$)sy
1178	1201	1101	1228	1118	α_w(C$_{20}$H$_{20}$C$_{21}$H$_{21}$C$_{22}$H$_{22}$C$_{23}$H$_{23}$C$_{24}$H$_{24}$C$_{25}$H$_{25}$C$_7$H$_7$ C$_8$H$_8$)sy
1142	1153	1057	1159	1055	υ_m(C$_{18}$C$_{19}$)sy+ υ_m(C$_{11}$NC$_{18}$)asy
1103	1132	1038	1122	1022	υ_w(C$_1$C$_2$ C$_3$ C$_4$C$_5$)sy
1021	1043	956	1053	959	π_m (C$_6$H$_6$C$_7$H$_7$ C$_8$H$_8$ C$_9$H$_9$)sy
963	973	892	982	894	υ_m (C$_{10}$C$_{11}$N)sy
815	832	762	808	736	α_m (C$_1$H$_1$C$_2$H$_2$C$_3$H$_3$C$_4$H$_4$C$_5$H$_5$)asy
769	712	652	730	665	α_m (C$_{13}$H$_{13}$C$_{14}$H$_{14}$C$_{15}$H$_{15}$C$_{16}$H$_{16}$C$_{17}$H$_{17}$)asy
697	501	459	485	441	υ_m (C$_{10}$FeC$_6$FeC$_9$FeC$_1$FeC$_4$Fe)sy
613	478	438	455	414	υ_m (C$_1$FeC$_2$FeC$_3$FeC$_4$FeC$_5$FeC$_6$Fe C$_7$FeC$_8$FeC$_9$Fe)sy
579	469	430	440	400	υ_m (C$_1$FeC$_2$FeC$_3$FeC$_4$FeC$_5$FeC$_6$Fe C$_7$FeC$_8$FeC$_9$Fe)sy

asy – asymmetric, Sy – symmetric, υ – stretching, π- in plane bending, α- out of plane bending, s - strong, m - medium. Scaling factor (6-311g++dp = 0.917 , lanl2dz=0.911)

3.5.1. C – H vibrations

Aromatic compounds commonly exhibit multiple weak bands in the region of 3100–3000 cm^{-1} due to aromatic C–H stretching vibration [28], in the title compounds there are benzenes and two cyclopentadienyl (Cp) rings as well, which appeared as symmetric and asymmetric stretching vibrational frequency in the range of 3100 -2837 cm^{-1} with both basis sets, as it's presented in the table 6, 7 and 8. moreover, other C-H stretching vibrations were lower in the range of 3008-2762cm-1. The methyl group of FPA appeared as asymmetric stretching vibration in 3008 cm^{-1} that was calculated using 6-311++G(d,p) and in 2964 cm^{-1} using LanL2DZ, However, the FPP's methyl group appeared in 2778cm^{-1} by 6-311++G(d,p) and in 2765 by LanL2DZ. The methylene bridges belonged to C$_{11}$ of title compounds were observed as symmetric and asymmetric stretching vibration in the range of 2990-2777cm^{-1}, moreover, the methylene bridge belonged to C13 of FPP appeared as symmetric in 2762 with 6-311++G(d,p) and in 2791cm^{-1} with LanL2dz.

The molecules had bending C-H as well. The methyl group and methylene bridges were observed as in plane bending vibration in the range of 1347-1416cm^{-1}, and as out of plane vibration in the range of 1153-1286cm^{-1}. The aromatic and cyclopentadienyl C-H out of plane bending vibrational frequency appeared in the range of 652-803 cm^{-1}.

The experimental bands for C-H stretching vibration appeared around 2360 cm^{-1} for FPA and 2159

cm^{-1} for FPP and FPB.

3.5.2. C =O vibrations

Organic chemists consider the C=O bond as a significant region. The carbonyl stretching vibrations in ketones are anticipated in the region 1715–1680 cm-1[29]. The carbon–oxygen double bond is formed by π– π bond, and the lone pair of electrons on oxygen also determines the nature of carbonyl group. The band caused by C=O stretching vibrations are observed in the region of 1637, 1573 and 1549cm^{-1} resulting from FPA, FPP and FPB respectively using 6-311++G(d,p), and in 1531, 1467 and 1443cm^{-1} for FPA, FPP and FPB respectively using LanL2DZ.

The carbonyl stretching vibration in experimental spectra for FPA, FPP and FPB are observed in the region of 1651, 1654 and 1639 cm^{-1} respectively.

3.5.3. C=C and C-C vibrations

The carbon-carbon stretching vibrations of aromatic ring are expected in the range of 1650 -1200 cm^{-1} [30]. In the title compounds, C–C bonds of aromatic rings had the strongest symmetric stretching vibrational frequencies in the frequency region of 1563, 1393, 1502 cm^{-1} that were obtained using 6-311 ++ G (d, p), likewise, in 1436, 1483 and 1504 cm^{-1} using LanL2dz, for FPA, FPP and FPB respectively. Indeed, it can be seen in experimental spectra that these bonds are located in 1593, 1592 and 1594 cm^{-1} for FPA, FPP and FPB respectively, which agreed with the calculated result. These bands match to C=C stretching vibrations.

Moreover, the C-C bonds correspond to the weakest frequencies of carbon-carbon stretching vibrations, which were calculated in the range of 1083,1053 and 1038 cm^{-1} that were computed using 6-311++G(d,p), and 1056, 1017 and 1022 cm^{-1} using LanL2DZ for the studied molecules FPA, FPP and FPB respectively. However, the experimental spectra show similar result in the range from 1023 to 1106 cm^{-1}.

3.5.4. C-N vibrations

It can be seen from the tables 6, 7 and 8, the bands at 1310/1237, 1296/1225/1128/1028 and 1257/1188/1057/892 cm^{-1} (6-311++G(d,p))for FPA, FPP and FPB respectively are assigned to C–N stretching vibration. These bands also appeared in similar region 1333/1230, 1283/1248/1129/1028 and 1267/1189/1055/ 894 cm^{-1} for FPA, FPP and FPB at LanL2DZ level.

The theoretically predicted scaled values show excellent agreement with experimental data.

3.5.5. Fe-Cp vibrations

The Fe-Cp stretching vibrational frequency are generally observed in the region of 700-400 cm^{-1}

[31, 32]. As it is expected, the Fe-Cp stretching vibrations appeared in the range of 433-399 cm^{-1}, whereas, the experimental results were in the range of 701-544cm^{-1}.

4.   NLO PROPERTIES

NLO effects arise from the interactions of electromagnetic fields in various media to produce new fields altered in phase, frequency, amplitude or other propagation characteristics from the incident fields [33]. Nonlinear optics has increasing attention due to its wide application in the area of laser technology, optical communication and data storage technology. Dipole moment gives an idea about the ionic character in a bond or a molecule. In general, larger the value of dipole moment more will be the ionic character. The value of dipole moment helps to predict the shape of the molecule. Polarizability and hyperpolarizability have been extensively applied in drug design [34]. A reliable prediction of NLO property requires adequate basis sets and therefore must involve both diffuse and polarization functions. As the basis becomes larger, one expects a better description of the compound and accordingly more accurate results [35]. In the view of these points, B3LYP/6-311G++(d,p) method has been used for the present study in order to see the effect of the level of theory and basis set. The equations are listed below.

Dipole moment is

$$\mu = (\mu^2_x + \mu^2_y + \mu^2_z)^{1/2}$$

Static polarizability

$$\alpha_{total} = 1/3 \ (\alpha_{xx} + \alpha_{yy} + \alpha_{zz})$$

Total polarizability is

$$\Delta\alpha = ((\alpha_{xx} - \alpha_{yy})^2 + (\alpha_{yy} - \alpha_{zz})^2 + (\alpha_{zz} - \alpha_{xx})^2/2)^{1/2}$$

First order hyperpolarizability is

$$\beta = (\beta^2_x + \beta^2_y + \beta^2_z)^{1/2}$$

Where:

$$\beta_x = \beta_{xxx} + \beta_{xyy} + \beta_{xzz}$$

$$\beta_y = \beta_{yyy} + \beta_{xxy} + \beta_{yzz}$$

$$\beta_z = \beta_{zzz} + \beta_{xxz} + \beta_{yyz}$$

In this work, the title compounds were fully optimized at B3LYP/6-311G++(d,p) method in the Gaussian 09 program. Theoretically, calculated values of dipole moment, polarizability (a) and hyperpolarizability (b) are shown in Table 9.

Table 9. The electric dipole moment, polarizability and first order hyperpolarizability of FPA, FPP and FPB

	FPA	FPP	FPB
Dipole moment			
μ_x	-1.9467	3.6761	-1.2079
μ_y	-3.3444	-0.8075	3.1877
μ_z	0.0471	-0.5939	0.5699
μ_{total}	3.8700	3.8103	3.4561
Polarizability (α)			
α_{xx}	279.757	276.062	355.475
α_{yy}	20.423	10.547	-8.796
α_{zz}	224.363	254.436	286.954
α_{xy}	-7.39	-16.022	-20.568
α_{xz}	-2.41	2.25	-12.281
α_{yz}	212.305	222.96	247.877
α_{total} **esu** ($\times 10^{-24}$)	35.3914	37.22083	43.98112
$\Delta\alpha$ **esu** ($\times 10^{-24}$)	9.426345	7.993513	14.9446
First order hyperpolarizability			
β_{xxx}	-133.9972	237.5609	141.6280
β_{xxy}	-138.8052	-28.6279	68.0773
β_{xyy}	-103.1344	-87.7888	-220.3617
β_{yyy}	-12.3554	-46.2432	82.6575
β_{xxz}	-48.3767	-65.9372	-72.0029
β_{xyz}	-8.5310	-3.0086	-22.8317
β_{yyz}	9.8797	-14.3753	17.5387
β_{xzz}	-1.1307	38.4404	-6.4932
β_{yzz}	-35.4540	-21.3817	23.0710
β_{zzz}	-0.0499	-8.8324	7.3038
β_{Totale} **esu** ($\times 10^{-33}$)	2635.671	1981.993	1721.225

5. FRONTIER MOLECULAR ORBITALS

The lowest-lying unoccupied molecular orbitals (LUMO) and the highest occupied molecular orbitals (HOMO) are known as frontier molecular orbitals (FMO). The HOMO represents the capacity to give an electron, while LUMO as an electron acceptor represents the capacity to acquire an electron. The energy gap between HOMO and LUMO decides the chemical reactivity, kinetic stability and, optical polarizability and chemical hardness–softness of a molecule [36, 37]. In the current study, the HOMO,

LUMO and the energy gap (ΔE) were calculated at both level of theory 6-311++G (d,p) and LanL2DZ. The energies and the contour diagrams of these molecular orbitals are shown in figure 10.

It can be seen from figure 8 that the HOMOs mainly concentrate on the ferrocenic part of the molecules, however, the LUMOs are distributed over the aromatic ring and the radical linked to the nitrogen atom except for the LUMO of FPP calculated by 6-311++G (d,p) is localized almost over the whole molecule. From the energy gap (ΔE) of the studied molecules, FPP is predicted to be the most reactive with least ΔE energy gap.
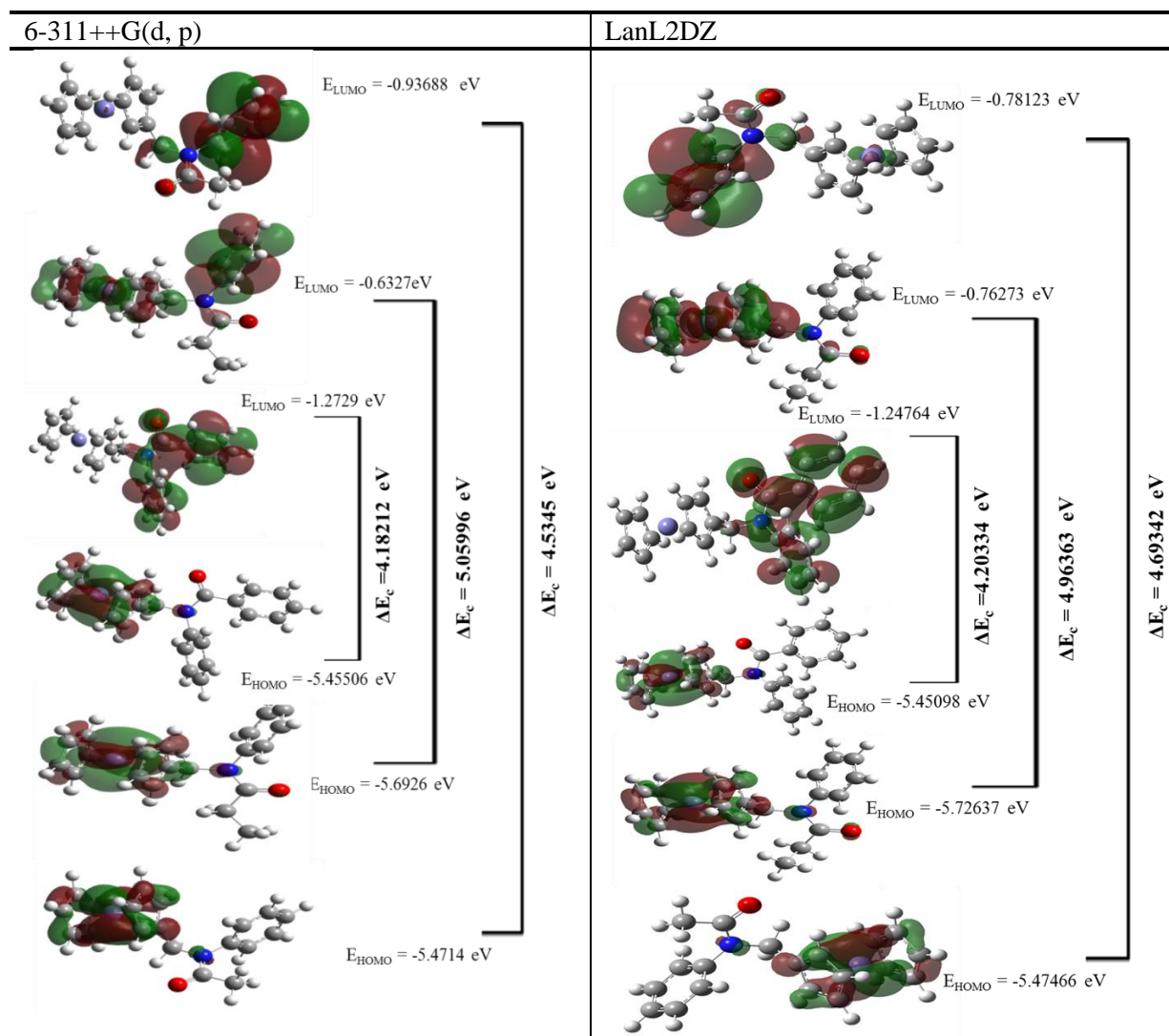
Fig. 6. Frontier molecular orbitals of FPA, FPP and FPB by DFT/B3LYP methods with 6-311++G(d, p) and LanL2DZ basis sets

6. CONCLUSION

A computational work in chemistry have not been carried out to examine the structural and spectroscopic properties of N-ferrocenylmethyl-N-phenylacetamide, N-ferrocenylmethyl-N-phenylpropionamide and N-ferrocenylmethyl-N-phenylbenzamide. Thus, the structure of the title molecules were studied using the theoretical methods of DFT / B3LYP with 6-311 ++G(d,p) and LanL2DZ basis sets.

After simulating the molecular structure of the candidate drugs with Gaussian 09 software and obtaining bond lengths and angles between its constituent atoms, a comparison with the experimental XRD data has shown a good agreement.

A vibrational analysis has been studied and functional groups were determined using both experimental and theoretical methods. Computational $_1$H and $_{13}$C chemical shift values were reported and compared with experimental data, showing good agreement for both 1H and 13C. HOMO and LUMO energy gaps explain the reactivity of FPA, FPP and FPB, where FPP were predicted to be the most reactive with least ΔE energy gaps. The MEP at the 6-311G++(d,p) optimized geometry was calculated to predict the reactive sites for electrophilic and nucleophilic attack for the studied molecules. Finally, the linear polarizability and first order hyperpolarizability of the studied molecules indicate that the compounds are good candidates of nonlinear optical materials.

7. ACKNOWLEDGEMENT

8. REFERENCES

[1] Kealy, T. and P. Pauson, Nature, 1951. 168. 1039.

[2] Wang, R., X. Hong, and Z. Shan, Tetrahedron letters, 2008. 49. 636. https://doi.org/10.1016/j.tetlet.2007.11.119

[3] Togni, A. and T. Hayashi, VCH Verlagsgessellschaft. 1995, 115. 540. https://doi.org/10.1002/recl.19961151012

[4] Sudhir, V.S., N.P. Kumar, and S. Chandrasekaran, Tetrahedron, 2010. 66. 1327. https://doi.org/10.1016/j.tet.2009.12.011

[5]Whittall, I.R., et al., ChemInform, 1998. 29.

[6] Bella, S.D., Chemical Society Reviews, 2001. 30 355. https://doi.org/10.1039/B100820J

[7] Hudson, R.D., Journal of Organometallic Chemistry, 2001. 637. 47.
https://doi.org/10.1016/S0022-328X(01)01142-1

[8] Constable, E.C., Angewandte Chemie International Edition in English, 1991. 30. 407.
https://doi.org/10.1002/anie.199104071

[9] Santis, G., Journal of the Chemical Society, Dalton Transactions, 1992. 22. 3283.
https://doi.org/10.1039/DT9920003283

[10] Beer, P.D., Jayne E.N, Mary E.H, Michael B.H, Journal of organometallic chemistry, 1992.
441. 465. https://doi.org/10.1016/0022-328X(92)80178-Z

[11] Beer, P.D. and D.K. Smith, Journal of the Chemical Society, Dalton Transactions, 1998.
417. https://doi.org/10.1039/A707278C

[12] Moore, A.J., et al., Journal of the Chemical Society, Chemical Communications, 1993. 4.
417. https://doi.org/10.1039/C39930000417

[13] Ahmedi, R. and T. Lanez, Journal of Fundamental and Applied Sciences, 2011. 3. 183.
https://doi.org/10.4314/jfas.v3i2.7

[14]Khelef, A., et al., Acta Crystallographica Section E: Structure Reports Online, 2012. 68.
m647. https://doi.org/10.1107/S1600536812016303

[15]   Khelef, A., M. Mahboub, and T. Lanez, IUCrData, 2016. 1. x160203.
https://doi.org/10.1107/S2414314616002030

[16] Khelef, A., Synthèse et étude du comportement anodique de quelques N-ferrocenyl-N-
phenylalkanamides et N'-ferrocenyl-N'-phenylalkanehydrazides et étude structurale de leurs
phases cristallines. Université Mohamed Khider Biskra. 2014.

[17] Frisch, M., et al., Inc., Wallingford, CT, 2009. 200. 28.

[18] Rahnamaye Aliabad, H. and M. Chahkandi, Zeitschrift für anorganische und allgemeine
Chemie, 2017. 643. 420. https://doi.org/10.1002/zaac.201600423

[19] Yáñez-S, M., et al., Computational and Theoretical Chemistry, 2017. 1118. 65.
https://doi.org/10.1016/j.comptc.2017.08.032

[20] Karabacak, M., et al., Spectrochimica Acta Part A: Molecular and Biomolecular
Spectroscopy, 2015. 136. 306. https://doi.org/10.1016/j.saa.2014.08.141

[21] Sarangani, T., S. Xavier, and S. Periandy, Journal of Molecular Structure, 2015. 1083. 39. https://doi.org/10.1016/j.molstruc.2014.11.035

[22] Ghosh, K., et al., Polyhedron, 2016. 112. 6. https://doi.org/10.1016/j.poly.2016.02.035

[23] Murray, J.S. and K. Sen, Molecular electrostatic potentials: concepts and applications. Elsevier. 1996.

[24] Lowdin, P.-O., Advances in quantum chemistry.Academic Press. 1979.

[25] Šponer, J. and P. Hobza, International Journal of Quantum Chemistry, 1996. 57. 959. https://doi.org/10.1002/(SICI)1097-461X(1996)57:5<959::AID-QUA16>3.0.CO;2-S

[26] Karabacak, M., et al., Spectrochimica Acta Part A: Molecular and Biomolecular Spectroscopy, 2012. 93. 33. https://doi.org/10.1016/j.saa.2012.02.110

[27] Belgacem, T., synthèse, cyclisation, étude electrochimique et structurale de quelques N-acyl-n'alkylférrocenyl méthyle hydrazide. university Elhadj Lakhder of batna. 2007.

[28] Varsányi, G., M.A.e. Kovner, and L. Láng, Assignments for vibrational spectra of 700 benzene derivatives. Budapest : Akademiai Kiado. 1973.

[29] Perkampus, H.H., LJ Bellamy. Berichte der Bunsengesellschaft für physikalische Chemie, 1976. 80. 99. https://doi.org/10.1002/bbpc.19760800121

[30]Demir, S., et al., Journal of Molecular Structure, 2016. 1108. 637. https://doi.org/10.1016/j.molstruc.2015.12.057

[31] Lippincott, E.R. and R.D. Nelson. The Journal of Chemical Physics, 1953. 21. 1307. Doi: 10.1063/1.1699202

[32] Noh, D.-Y., et al., Polyhedron, 2001. 20. 1939. https://doi.org/10.1016/S0277-5387(01)00783-5

[33] Sun, Y.-X., et al., Journal of Molecular Structure: THEOCHEM, 2009. 904. 74. https://doi.org/10.1016/j.theochem.2009.02.036

[34] Wang, J., et al., The Journal of Physical Chemistry A, 2007. 111. 4443. https://doi.org/10.1021/jp068423w

[35] Xavier, R.J. and P. Dinesh, Spectrochim Acta A Mol Biomol Spectrosc, 2014. 118. 999. https://doi.org/10.1016/j.saa.2013.09.120

[36] Asiri, A.M., et al., Spectrochimica Acta Part A: Molecular and Biomolecular Spectroscopy, 2011. 82. 444. https://doi.org/10.1016/j.saa.2011.07.076

[37] Kosar, B. and C. Albayrak, Spectrochimica Acta Part A: Molecular and Biomolecular Spectroscopy, 2011. 78. 160. https://doi.org/10.1016/j.saa.2010.09.016